Electron paramagnetic resonance and optical properties of Cr^{3+} doped $YAl_3(BO_3)_4$

2003 J. Phys.: Condens. Matter 15 539

(http://iopscience.iop.org/0953-8984/15/3/318)

INSTITUTE OF PHYSICS PUBLISHING JOURNAL OF PHYSICS: CONDENSED MATTER

J. Phys.: Condens. Matter **15** (2003) 539–547 PII: S0953-8984(03)40028-3

Electron paramagnetic resonance and optical properties of Cr^{3+} doped $YAl_3(BO_3)_4$

Jon-Paul R Wells[1,5], Mitsuo Yamaga[2], Thomas P J Han[3] and Makoto Honda[4]

[1] Department of Physics and Astronomy, University of Sheffield, Sheffield S3 7RH, UK
[2] Department of Mathematical and Design Engineering, Gifu University, Gifu 501-1193, Japan
[3] Department of Physics, University of Strathclyde, Glasgow G1 1XN, UK
[4] Faculty of Science, Naruto University of Education, Naruto 772-8502, Japan

E-mail: j.p.wells@sheffield.ac.uk

Received 29 July 2002, in final form 7 November 2002
Published 13 January 2003
Online at stacks.iop.org/JPhysCM/15/539

Abstract

We report on the electron paramagnetic resonance (EPR) and optical absorption and fluorescence spectroscopy of $YAl_3(BO_3)_4$ single crystals doped with 0.2 mol% of trivalent chromium. From EPR we determine that the Cr^{3+} ions reside in sites of essentially octahedral symmetry with an orthorhombic distortion. The ground state $^4A_2$ splitting is determined to be $2\sqrt{D^2+3E^2} \approx 1.05 \pm 0.04\ cm^{-1}$, where D and E are fine-structure parameters, and we can attribute this splitting to the combined effect of a low-symmetry distortion and spin–orbit coupling. The g-values and fine-structure parameters D and E of the ground state $^4A_2$ are measured to be $g_x \approx g_y \approx g_z = 1.978 \pm 0.005$, $|D| = 0.52 \pm 0.02\ cm^{-1}$ and $|E| = 0.010 \pm 0.005\ cm^{-1}$ respectively. From 10 K optical absorption we have measured the position and crystal-field splittings of the ^2E, $^2T_1$, $^4T_2$, $^2T_2$ and $^4T_1$ states with the $^4T_2$ and $^4T_1$ levels appearing as vibronically broadened bands.

1. Introduction

Self-frequency-doubling crystals doped with rare-earth or transition-metal ions have attracted considerable interest from the scientific community because of the promise of solid state lasers employing intra-cavity, self frequency doubling. Amongst these materials, double borate crystals of the type $RX_3(BO_3)_4$ have been extensively studied [1–7]. In a series of papers, Wang *et al* have studied the growth and spectroscopic properties of Cr^{3+} [8–10] doped $YAl_3(BO_3)_4$ (YAB), $GdAl_3(BO_3)_4$ (GAB), $YSc_3(BO_3)_4$ (YSB) and $GdSc_3(BO_3)_4$ (GSB) and Ti^{3+} [11, 12] doped YAB and GAB. These studies show that the transition-metal ion occupies a trigonally

[5] Author to whom any correspondence should be addressed.

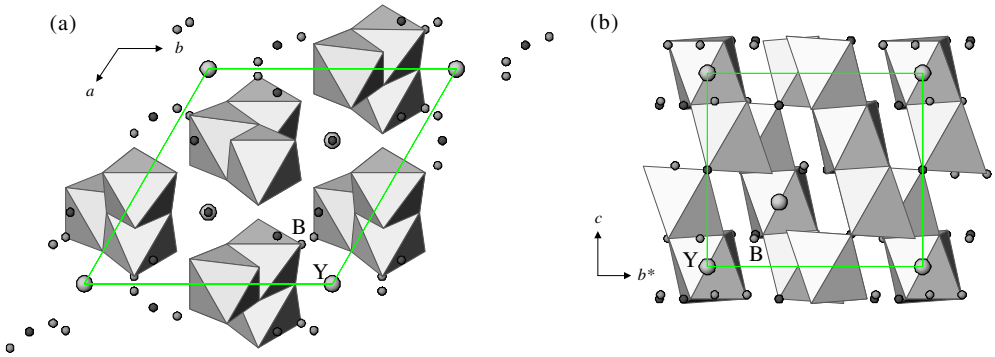

Figure 1. Crystal structure of YAB: (a) projection to the (0001) plane along the *c*-axis and (b) projection to the $(10\bar{1}0)$ plane along the *a*-axis. The Al ions are located at the centre of an octahedron. Y and B ions are denoted by large and small solid circles respectively.

(This figure is in colour only in the electronic version)

distorted Al^{3+}/Sc^{3+} octahedral site with broadband Cr^{3+} $^4T_2 \rightarrow {}^4A_2$ fluorescence observed for the scandium based borates and sharp 'R' $^2E \rightarrow {}^4A_2$ fluorescence observed for the aluminium based compounds corresponding to weak and strong octahedral field sites, respectively.

Rare-earth doped borates such as YAB containing Nd^{3+} [13, 14] and Er^{3+} [15] have also been investigated. In this case, dopant ions occupy the trivalent yttrium site at the centre of a trigonally coordinated oxygen prism giving a point group symmetry at the rare-earth site of D_3. More recently, emphasis has been upon the YAB:Yb^{3+} system [16]. Lasing powers of 1.1 W of CW green output have been obtained via diode end pumping with an optical conversion efficiency up to 10% [17].

Despite the large number of publications relating to YAB:Cr^{3+}, as yet a comprehensive report of its spectroscopic properties is lacking. We present new results on the electron paramagnetic resonance (EPR) of YAB:Cr^{3+} which we have used to measure the $^4A_2$ ground state zero-field splitting, the ground state magnetic splitting factors and fine-structure parameters. To complement these ground state measurements, we have measured the 10 K and room-temperature absorption and fluorescence spectra. The temperature dependent population decay rates and 'R' lineshift have been studied recently by Dominiak-Dzik *et al* [18]. Our own investigations of these properties are in general agreement with the findings of [18] and we will not present them in detail here. We have also measured the temperature dependent R_1 fluorescence linewidth which we interpret in terms of a commonly employed phonon scattering model.

2. Experimental details

The YAB crystal is reported to have trigonal crystal structure with the *R*32 space group [19]. The parameters of the trigonal cell are $a = b = 9.295$ Å and $c = 7.243$ Å.The unit cell is shown in figure 1. An octahedron consists of a central Al^{3+} ion and six nearest-neighbour O^{2-} ligand ions. There are three Al^{3+} octahedra in the unit cell, which have trigonal symmetry about the *c*-axis. Cr^{3+} ions substitute preferentially for Al^{3+} ions because the ionic radius (0.62 Å) of Cr^{3+} is close to that (0.53 Å) of Al^{3+}.

The YAB:0.2% Cr^{3+} crystal used in this study was grown using the high-temperature top seeded solution growth technique [8–10]. Oriented samples were prepared for EPR and polarized optical absorption measurements using Laue x-ray diffraction.

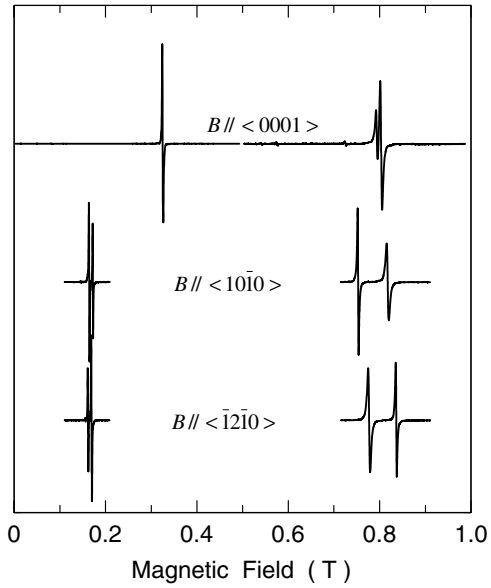

Figure 2. The EPR spectra of Cr^{3+} in YAB measured at 293 K with a microwave frequency $\nu = 9.061$ GHz and $B \parallel \langle 0001 \rangle$ and with $\nu = 9.075$ GHz and $B \parallel \langle 10\bar{1}0 \rangle$, and $\langle \bar{1}2\bar{1}0 \rangle$.

Absorption spectra were recorded with an AVIV associates 14DS double-beam spectrometer with crystals cooled to a base temperature of 10 K using a Leybold cryogenic refrigeration unit. Laser excitation and fluorescence spectra were recorded using a 4 W Coherent Innova 70 argon ion laser to optically pump a Spectra-Physics 375B dye laser. DCM dye was used for the excitation of Cr^{3+} in these materials. The sample was cooled with a CTI-Cryogenics model 22C cryogenic refrigerator and temperature variability was maintained by a Palm Beach Cryogenics temperature controller. Fluorescence was recorded using a SPEX 500M single monochromator with a Hamamatsu R9249 photomultiplier, which was thermoelectrically cooled to $-25\,^{\circ}$C, and was used to detect the light.

The EPR measurements were carried out using a JES-FA200 X-band spectrometer with microwave frequencies of 9.060–9.077 GHz at room temperature and a Bruker EMX10/12 X-band spectrometer with 9.677–9.690 GHz in the temperature range of 3–20 K. Both spectrometers employ 100 kHz field modulation.

3. Electron paramagnetic resonance

Figure 2 shows the EPR spectra for the YAB:Cr^{3+} crystal measured at a microwave frequency of 9.061 GHz with magnetic fields $\boldsymbol{B} \parallel \langle 0001 \rangle$, $\langle 10\bar{1}0 \rangle$ and $\langle \bar{1}2\bar{1}0 \rangle$ crystallographic directions. One milliWatt of microwave power was incident upon the cavity and the measurements were made at 293 K. The EPR spectrum for $B \parallel \langle 0001 \rangle$ consists of intense resonance lines at 0.326, 0.793 and 0.803 T. A splitting of the lines, apparent at $\sim$0.80 T, is due to a misalignment between the crystalline $\langle 0001 \rangle$ axis and the magnetic field which we estimate to be less than 2°. In the cases of $B \parallel \langle 10\bar{1}0 \rangle$ and $\langle \bar{1}2\bar{1}0 \rangle$, the splitting of the resonance lines at $\sim$0.18 and $\sim$0.80 T is altogether too large to be assigned as a misalignment and is ascribed to orthorhombic distortions of the Cr^{3+} centre. In the case of a small zero-magnetic-field splitting compared with the microwave frequency, the typical pattern consists of three resonance lines due to a

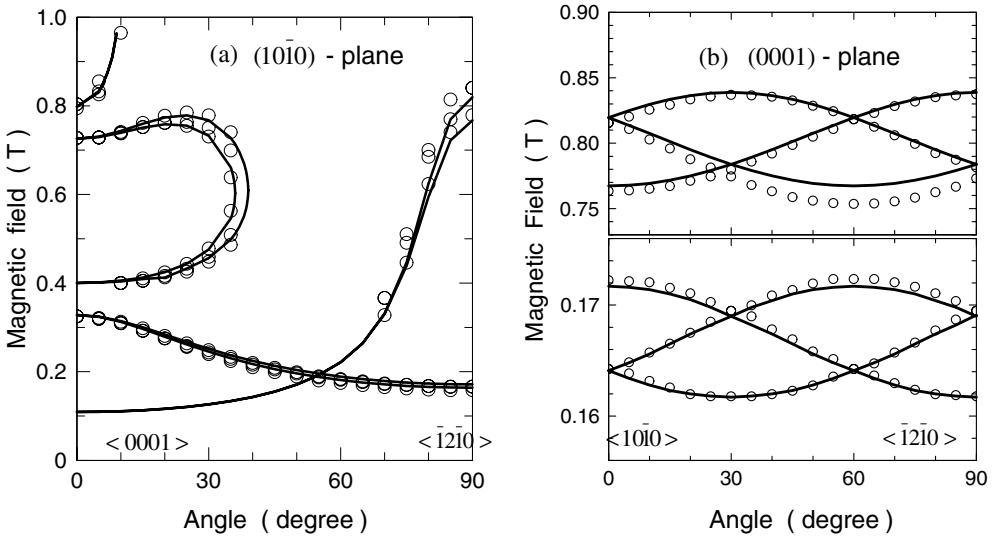

Figure 3. The angular variation of the EPR resonance lines in (a) the (10$\bar{1}$0)-plane and (b) the (0001)-plane measured at 293 K. The open circles represent experimental data points. The solid curves are calculated using equation (1) and the spin-Hamiltonian parameters (see text).

central $|\frac{1}{2}\rangle \leftrightarrow |-\frac{1}{2}\rangle$ transition and two fine-structure $|\pm\frac{1}{2}\rangle \leftrightarrow |\pm\frac{3}{2}\rangle$ transitions located nearly evenly, either side of the central line at ∼0.33 T [20]. However, the observed EPR spectra are not consistent with this, suggesting that the zero-field splitting is larger than the microwave frequency.

The angular variation of the Cr^{3+} resonance lines in the YAB crystal at 293 K is plotted in figure 3 for magnetic field rotations in (a) the (10$\bar{1}$0)-plane and (b) the (0001)-plane. As shown in figure 3(a), the intense curves at 0.326 and 0.794 T and two weak curves at 0.398 and 0.733 T observed for $B \parallel \langle 0001 \rangle$ are split into three curves when the magnetic field is applied away from $\langle 0001 \rangle$. In the same way, low- and high-field components of the EPR spectra in the (0001)-plane as shown in figure 3(b) consist of three curves with a 120° period. These angular variations indicate that there are three magnetically inequivalent Cr^{3+} centres with orthorhombic symmetry in the YAB crystal. This result is consistent with three Al^{3+} octahedra in the unit cell in figure 1.

The dependence of the EPR spectra upon magnetic-field orientation (figure 3) can be analysed using an effective spin Hamiltonian appropriate to orthorhombic symmetry [21], i.e.

$$H = \mu_B g_z B_z S_z + \mu_B g_x B_x S_x + \mu_B g_y B_y S_y + D(S_z^2 - \tfrac{1}{3}S(S+1)) + E(S_x^2 - S_y^2) \qquad (1)$$

where $S = \frac{3}{2}$ for the Cr^{3+} ion, D and E are fine-structure parameters and μ_B is the Bohr magneton. The principal z-, x- and y-axes, respectively, of the spectra are the $\langle 0001 \rangle$, $\langle 10\bar{1}0 \rangle$ and $\langle \bar{1}2\bar{1}0 \rangle$ directions of the crystal. The solid curves shown in figures 3(a) and (b) are calculated using equation (1) and the spin-Hamiltonian parameters of $g_x \approx g_y \approx g_z = 1.978 \pm 0.005$, $|D| = 0.52 \pm 0.02$ cm^{-1} and $|E| = 0.010 \pm 0.005$ cm^{-1}. These are in good agreement with the experimental data points.

In order to determine the sign of D, the EPR spectra of Cr^{3+} with $\boldsymbol{B} \parallel \langle 0001 \rangle$, $\langle 10\bar{1}0 \rangle$ and $\langle \bar{1}2\bar{1}0 \rangle$ were measured in the temperature range of 3–20 K. As the relative integrated intensities of the EPR lines of Cr^{3+}:YAB do not change with temperature, no conclusive results could be obtained and the sign of D is as yet undetermined.

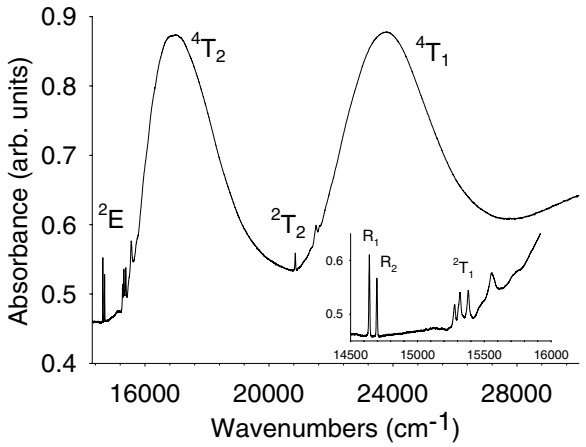

Figure 4. 10 K absorption spectrum of YAB:0.2% Cr^{3+}. Inset: expanded view of the $^4A_2 \rightarrow {}^2E$ and $^2T_1$ transitions in the range of 14 500–16 000 cm^{-1}.

4. Absorption and fluorescence

Previous studies have reported the absorption spectra of YAB:Cr^{3+} at room temperature only [6]. The 10 K absorption spectrum of YAB:0.2% Cr^{3+} is shown in figure 4. The dominant features are the broad bands due to the spin allowed $^4A_2(t_2^3e) \rightarrow {}^4T_1(t_2^2e)$ and $^4T_2(t_2^2e)$ transitions centred at 23 750 and 16 950 cm^{-1} respectively. Since the initial and final states of these transitions are derived from different crystal-field orbitals, the energy separations are very sensitive to the value of the cubic crystal-field parameter (Dq). In consequence, the transitions are characterized by large values of the Huang–Rhys parameter. Sharp $^4A_2 \rightarrow {}^2E$ 'R' line structure is observed indicating that the Cr^{3+} ions experience a strong crystal field with $Dq/B > 2.3$ [10]. A twofold ^2E splitting is observed with transition frequencies of 14 641 and 14 695 cm^{-1}. In the inset to figure 4, the R lines are shown to have a 3:4 (R_2:R_1) intensity ratio. The 54 cm^{-1} splitting of the R lines at 10 K is attributable to the combined action of a trigonal distortion and spin–orbit coupling which splits the ^2E states (and the $^4A_2$ ground state, which is split by 1.0 cm^{-1}—see section 3 above) into Kramers doublets. Three moderately sharp transitions at 15 276, 15 321 and 15 376 cm^{-1} are assigned as the $^4A_2 \rightarrow {}^2T_1$ transitions. An additional transition at 20 846 cm^{-1} is assigned as an $^4A_2 \rightarrow {}^2T_2$ transition. See table 1.

Figure 5 shows the polarized absorption spectra measured at room temperature. The σ and π polarization geometries are defined as being when the electric field vector of the light is perpendicular and parallel to the c-axis respectively. The σ-component of the $^4T_1$ band is 1.5 times larger than the π-component, whereas the σ- and π-components of the $^4T_2$ band are comparable to each other. Although a difference in the peak energy for the $^4T_1$ band is not obvious, the peak of the σ-component of the $^4T_2$ band is shifted to low energy compared with that of the π-component. Comparing these results with that in ruby (Cr^{3+}:Al_2O_3) [22], we find that in the case of ruby the $^4T_1\pi$- and $^4T_2\sigma$-components are dominant. This is in agreement with the predicted polarization behaviour when induced by the z-component of a T_{1u} odd-parity static distortion of the Cr^{3+} complex. As the polarization of the $^4T_1$ band in Cr^{3+}:YAB is the reverse of that observed in ruby, it is expected that a T_{2u} odd-parity static distortion of the Cr^{3+} complex is created predominantly along the z-axis. The additional observation that the σ- and π-components of the $^4T_2$ band are comparable to each other indicates that the x- and y-components of T_{2u} odd-parity static distortion should be included [23]. This is consistent

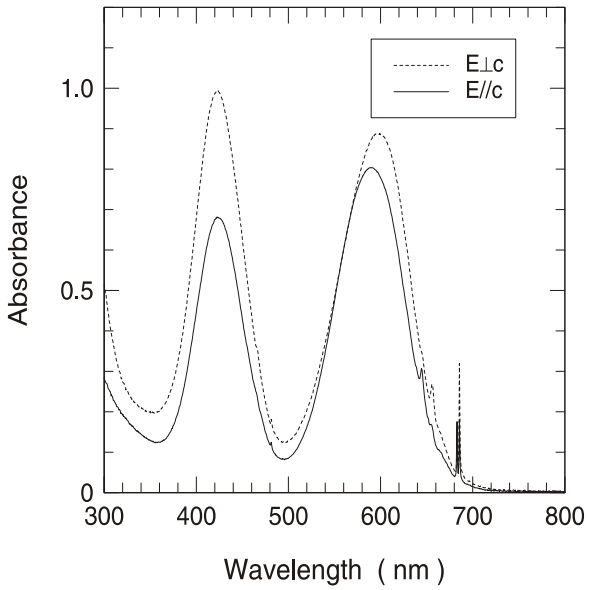

Figure 5. 300 K polarized absorption spectrum of YAB:0.2% Cr^{3+}.

Table 1. 10 K energy levels (± 1 cm^{-1}) for YAB:0.2% Cr^{3+}. The values in round brackets are the broadband peaks.

State	Energy
$^4A_2$	0
	1.05
^2E	14 641
	14 695
$^2T_1$	15 275
	15 321
	15 375
$^4T_2$	(16 950)
$^2T_2$	20 846
$^4T_1$	(23 750)

with the fact that the Cr^{3+} complex in YAB has orthorhombic symmetry as determined from the EPR analyses. Yamaga *et al* have calculated the polarization of the $^4T_2$ band of Cr^{3+} under trigonal symmetry, being induced by T_{1u} and T_{2u} odd-parity static distortions [23]. According to their calculation, the σ- and π-components of the $^4T_2$ band are largely attributable to the ^4E and $^4A_1$ levels of the $^4T_2$ excited state respectively. The shift of the σ-component to lower energy indicates that the ^4E level is lower in energy than the $^4A_1$ level.

Figure 6 shows the 10 and 300 K fluorescence of YAB:0.2% Cr^{3+}. At both 10 and 300 K sharp R line emission is observed which is accompanied by Stokes and anti-Stokes shifted phonon sideband structure to the low-and high-energy sides of the R lines, respectively. In the 300 K spectrum these transitions are superimposed upon a broadband structure. We can attribute this to the Stokes shifted fluorescence of the $^4T_2$ states, a phenomenon observed for other crystals with $^4T_2 \rightarrow {}^2E$ separations in the range 400–1000 cm^{-1} (see for example the

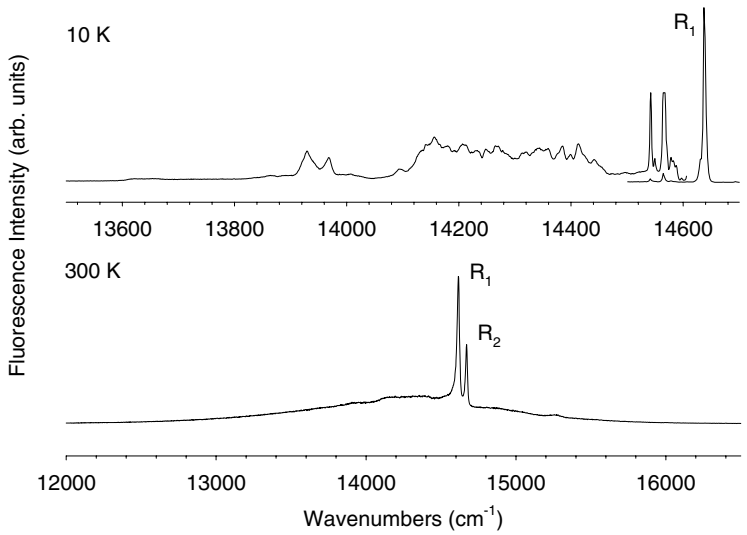

Figure 6. 10 and 300 K fluorescence spectra.

case of YAG:Cr^{3+} [24, 25]). These $^4T_2$ transitions are observable due to the thermal occupancy of these states at room temperature, whose $^4T_2 \rightarrow {}^4A_2$ transition moments are several orders of magnitude greater than those of the $^2E \rightarrow {}^4A_2$ transitions. The linewidths of the Cr^{3+} R lines in ionic crystals can be thought of as comprised of temperature dependent and temperature independent components. At the lowest temperatures, we may think of the R lines as broadened due to strains produced during crystal growth, that is, strain fields set up by impurity ions or intrinsic disorder within the compound. In other words, the linewidth is dominated by inhomogeneous broadening at 10 K. This is essentially a temperature independent process from which a constant linewidth can be derived. The $\sim$2.5 cm^{-1} linewidth observed for these strong-field $^4A_2 \leftrightarrow {}^2E$ transitions is similar to those for other ordered crystals (e.g. the spinels, $MgAl_2O_4$:Cr^{3+} and $ZnAl_2O_4$:Cr^{3+} [26]) which are typically of the order of 1 cm^{-1}. By contrast, the 'R' lines observed in substitutionally disordered materials have a considerably greater contribution from inhomogeneity with linewidths that vary widely from tens up to a hundred wavenumbers at cryogenic temperatures. Examples are $Ca_3Ga_2Ge_4O_{14}$:Cr^{3+} [27] which has an R_1 linewidth of $\sim$20 cm^{-1} or $CaYAlO_4$:Cr^{3+} [28] with an R_1 linewidth of $\sim$100 cm^{-1}.

Homogeneous line-broadening will give rise to a temperature dependent linewidth contribution, a common source of which is the two-phonon Raman dephasing process [29, 30]. We can model the temperature dependent linewidth of the 14 641 cm^{-1} R_1 line in terms of this interaction as follows:

$$\Gamma(T) = \Gamma(0) + A_W \left(\frac{T}{T_D}\right)^7 \int_0^{T_D/T} \frac{x^6 e^x}{(e^x - 1)^2}\, dx \tag{2}$$

where A_W is an effective coupling constant. Employing the 10 K linewidth of 2.5 cm^{-1} as an approximation to $\Gamma(0)$ and treating A_W and the Deybe temperature ($T_D = \hbar\omega/k$) as free parameters we obtain the fit to the temperature dependent linewidth as shown in figure 7 as a solid line with the experimental points shown as filled circles. The best fit was obtained for a Deybe temperature of 500 K and an effective coupling constant of 150 cm^{-1}. This value is comparable to that obtained for YAG:Cr^{3+} of 233 cm^{-1} [31].

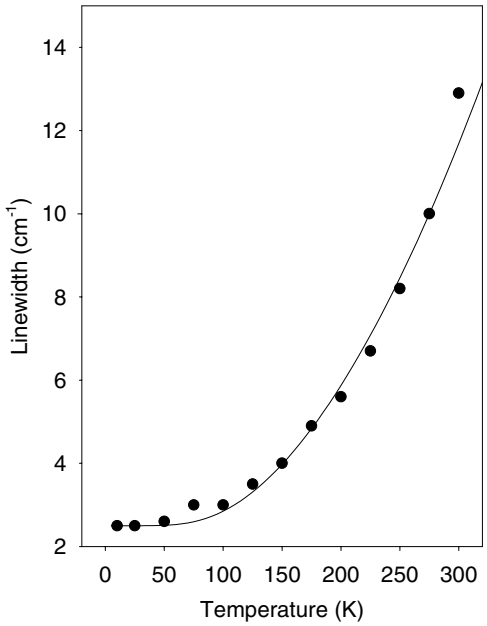

Figure 7. The temperature dependent R_1 linewidth. The solid curve is a calculation based upon equation (2) with $T_D = 500$ K and $A_W = 150$ cm^{-1} (see text).

5. Concluding remarks

From EPR measurements we have determined the symmetry of the Cr^{3+} centre in YAB to be essentially octahedral with an orthorhombic distortion. This distortion of the Cr^{3+} octahedron is the same as that of a Ti^{3+} octahedron in YAB except that the principal z-axis is tilted by seven degrees from the c-axis [11]. These Cr^{3+} and Ti^{3+} centres show large orthorhombic distortions which are different from the trigonal distortion of Al^{3+} octahedra in pure YAB crystals. This difference is due to the wavefunctions of the d orbitals of Cr^{3+} and Ti^{3+} ions. The lobes of the wavefunctions lower the symmetry of the octahedra through interaction with the lattice ions. As the ground state of Cr^{3+} is represented by $^4A_{2g}$ (t_{2g}^3), the low-symmetry distortion (which adds to the intrinsic trigonal distortion) is smaller than that of Ti^{3+}.

The g-values and fine-structure parameters of Cr^{3+} in YAB are measured to be $g_x \approx g_y \approx g_z = 1.978$, $|D| = 0.52$ cm^{-1} and $|E| = 0.010$ cm^{-1} respectively. The $^4A_2$ ground state splitting is inferred as 1.05 cm^{-1} which is largely attributable to the low-symmetry orthorhombic distortion. Such a distortion strongly affects the polarization of the optical spectra of Cr^{3+}, which depend upon the symmetry of the wavefunctions of the ground and excited states. The shift of the σ-component of the $^4T_2$ absorption band to lower energy indicates that the $^4E(^4T_2)$ excited state is lower in energy than the $^4A_1(^4T_2)$ level. This energy splitting is the same as that of ruby with the result that the principal axis of the Cr^{3+} octahedron is compressed along the c-axis. This result is consistent with the crystal structure of YAB [11, 19]. The observed polarization dependence of the absorption spectra is dominated by a T_{2u} odd parity distortion of the Cr^{3+} complex along the crystallographic z-axis with smaller contributions from the x-and y-components. This is consistent with the orthorhombic symmetry of the Cr^{3+} site in YAB as determined by the EPR results. Further optical absorption and fluorescence studies show the presence of a single strong-field Cr^{3+} site with sharp R lines

split by 54 cm^{-1}. A phonon scattering model accounts for the temperature dependent linewidth of the R_1 line.

Acknowledgment

The authors would like to thank Professor N Kodama for information regarding the crystallographic structure of YAB.

References

[1] Huang Y D and Luo Z D 1994 *Opt. Commun.* **112** 101
[2] Iwai M, Mori Y, Sasaki T, Nakai S, Sarukura N, Liu Z L and Segawa Y 1995 *Japan. J. Appl. Phys.* **34** 2338
[3] Wang G, Han T P J, Gallagher H G and Henderson B 1995 *Appl. Phys. Lett.* **67** 3906
[4] Jung S T, Yoon J T and Chung S J 1996 *Mater. Res. Bull.* **31** 1021
[5] Pan H F, Wang P, Fan X F, Wang R H and Lu B S 1996 *Chin. Phys. Lett.* **13** 1021
[6] Dianov E M, Dmitruk M V, Karasik A Ya, Kirpichenova E O, Osiko V V, Ostroumov V G, Timoshechkin M I and Shcherbakov I A 1980 *Sov. J. Quantum Electron.* **10** 1222
[7] Tsuboi T and Ter-Mikirtychev V V 1996 *Phys. Status Solidi* b **198** K5
[8] Wang G, Gallagher H G, Han T P J and Henderson B 1995 *J. Cryst. Growth* **153** 169
[9] Wang G, Gallagher H G, Han T P J and Henderson B 1995 *Radiat. Eff. Defects Solids* **136** 953
[10] Wang G, Gallagher H G, Han T P J and Henderson B 1996 *J. Cryst. Growth* **163** 272
[11] Wang G, Gallagher H G, Han T P J, Henderson B, Yamaga M and Yosida T 1997 *J. Phys.: Condens. Matter* **9** 1649
[12] Wang G, Han T P J, Gallagher H G and Henderson B 1997 *J. Cryst. Growth* **181** 48
[13] Jaque D, Capmany J, Molero F and Garcia-Sole J 1998 *Appl. Phys. Lett.* **73** 3659
[14] Jaque D, Campany J, Luo Z D and Garcia-Sole J 1997 *J. Phys.: Condens. Matter* **9** 9715
[15] Beregi E, Hartmann E, Malicsko L and Madarasz J 1999 *Cryst. Res. Technol.* **34** 641
[16] Jiang H, Li J, Wang J, Hu X-B, Liu H, Teng B, Zhang C-Q, Dekker P and Wang P 2001 *J. Cryst. Growth* **233** 248
[17] Dekker P, Dawes J M, Piper J A, Liu Y and Wang J 2001 *Opt. Commun.* **195** 431
[18] Dominiak-Dzik G, Ryba-Romanowski W, Grinberg M, Beregi E and Kovacs L 2002 *J. Phys.: Condens. Matter* **14** 5229
[19] Ballman A A 1962 *Am. Mineral* **47** 138
[20] Yamaga M, Henderson B, Holliday K, Yosida T, Fukui M and Kindo K 1999 *J. Phys.: Condens. Matter* **11** 10497
[21] Pilbrow J R 1990 *Transition Ion Electron Paramagnetic Resonance* (Oxford: Clarendon) p 120
[22] Henderson B and Imbusch G F 1989 *Optical Spectroscopy of Inorganic Solids* (Oxford: Oxford University Press)
[23] Yamaga M, Henderson B and O'Donnell K P 1990 *J. Lumin.* **46** 397
[24] Wall W A, Karpick J T and Di Bartolo B 1971 *J. Phys. C: Solid State Phys.* **4** 3258
[25] Hehir J P, Henry M O, Larkin J P and Imbusch G F 1974 *J. Phys. C: Solid State Phys.* **7** 2241
[26] Wood D L, Imbusch G F, Macfarlane R M, Kisliuk P and Larkin D M 1968 *J. Chem. Phys.* **48** 5255
[27] Macfarlane P I, Han T P J, Henderson B and Kaminskii A A 1994 *Opt. Mater.* **3** 15
[28] Yamaga M, Macfarlane P I, Holliday K, Henderson B, Kodama N and Inoue Y 1996 *J. Phys.: Condens. Matter* **8** 3487
[29] McCumber D E and Sturge M D 1963 *J. Appl. Phys.* **34** 1682
[30] Powell R C 1998 *Physics of Solid State Laser Materials* (New York: American Institute of Physics)
[31] Vink A P 2000 *PhD Thesis* Utrecht University